

# Antibacterial and Water Purification Activities of Self-Assembled Honeycomb Structure of Aerosol Deposited Titania Film

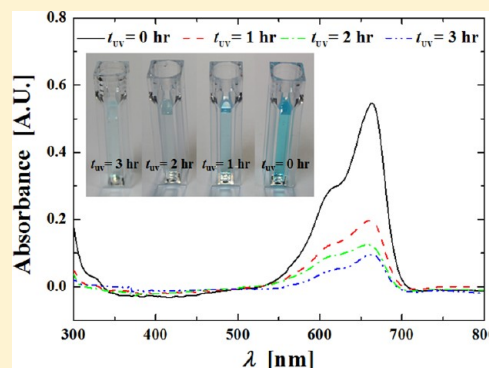
Jung-Jae Park,<sup>†</sup> Jong-Gun Lee,<sup>†</sup> Do-Yeon Kim,<sup>†</sup> Joo-Hyun Hong,<sup>‡</sup> Jae-Jin Kim,<sup>‡</sup> Seungkwon Hong,<sup>§</sup> and Sam S. Yoon<sup>†,\*</sup>

<sup>†</sup>School of Mechanical Engineering, Korea University, Seoul, 136-713 Korea

<sup>‡</sup>Division of Environmental Science and Ecological Engineering, Korea University, Seoul, 136-713 Korea

<sup>§</sup>School of Civil, Environmental and Architectural Engineering, Korea University, Seoul 136-713, Korea

**ABSTRACT:** A simple and rapid room-temperature aerosol deposition method was used to fabricate TiO<sub>2</sub> films for photokilling/photodegradation applications. TiO<sub>2</sub> particles were accelerated to supersonic speeds and fractured upon impacting a glass substrate to form a functional thin film, a process known as aerosol deposition. After deposition, the films were annealed at various temperatures, and their photokilling/photodegradation performances following ultraviolet (UV) exposure were evaluated by counting the number of surviving bacterial colonies, and by a methylene blue decolorization test. The photocatalytic performances of all TiO<sub>2</sub> films were obtained under weak UV exposure (0.6 mW/cm<sup>2</sup>). The film density, crystalline phase, and surface roughness (morphology) were measured by scanning electron microscopy, X-ray diffraction, UV-visible spectroscopy, and atomic force microscopy. The unique, self-assembled honeycomb structure of the aerosol deposited films contributed to the increase in surface area because of extreme roughness, which enhances the photokilling and photodegradation performance. Nonannealed films yielded the best photocatalytic performance due to their small crystalline sizes and large surface areas due to increased surface roughness.



## 1. INTRODUCTION

Titania (TiO<sub>2</sub>, anatase) is a semiconductor with a bandgap value of 3.2 eV.<sup>1</sup> Since the discovery of the electrochemical photolysis of water on a titania electrode by Fujishima and Honda in 1972,<sup>2</sup> TiO<sub>2</sub> has been used in numerous applications, such as dye-sensitized solar cells, self-cleaning products, water and air purification,<sup>3</sup> medical applications,<sup>4–6</sup> odor elimination, decoloring wastewater,<sup>7–12</sup> mineralization of both hazardous organic and inorganic materials,<sup>13–16</sup> soil decontamination,<sup>17</sup> destruction of cancer cells and viruses,<sup>18</sup> and medical sterilization.

Photocatalytically generated reactive oxygen species like hydroxyl radicals, hydrogen peroxide, and superoxide can work together to decompose or oxidize various organic and inorganic compounds.<sup>19–22</sup> Titania's strong oxidizing capabilities are especially useful in water purification applications and are economically viable and environmentally friendly. TiO<sub>2</sub> catalyst can be recycled indefinitely and requires no additional chemical treatment.<sup>23,24</sup>

Because photocatalysis is an interfacial phenomenon,<sup>25</sup> maximum disinfection performance is achieved when the active surface-area-to-volume ratio is maximized, thereby facilitating efficient UV irradiance and high quantum yield.<sup>26</sup> A mobilized mode that suspends TiO<sub>2</sub> powders in aqueous media inside a fluidized reactor can maximize performance.<sup>27</sup> However, this mobilized mode ultimately requires separation of the fine TiO<sub>2</sub> powder from the purified water; this is difficult because fine

powders remain in a colloidal state and do not sufficiently settle – additional equipment is required.<sup>28</sup> To circumvent this technological difficulty, an immobilized mode for TiO<sub>2</sub> photocatalysis is often proposed as an alternative; it necessitates permanent adhesion of TiO<sub>2</sub> powder on supporting materials such as quartz, fiber-mat, mesh, stainless steel, etc. There is also a pseudoimmobilized mode for various photocatalytic degradation processes, which uses a TiO<sub>2</sub>-coated fiberglass mesh,<sup>23</sup> quartz sand particles,<sup>27</sup> activated carbon,<sup>29</sup> or magnetic powder.<sup>30</sup> These pseudoimmobilized modes take advantage of the larger size of TiO<sub>2</sub>-coated beads, which enables the retention of a reasonably large surface-area-to-volume ratio. Simultaneously, beads are large enough to be easily separated from the treated water.

Although an immobile process, TiO<sub>2</sub> films are favorable because of their simple and inexpensive manufacturability. Furthermore, such film-based (immobilized mode) disinfection technologies have certain advantages over fluidized-bed-based technology (mobilized mode), because these film-based modes can take advantage of “free” sunlight as a UV source, whereas a fluidized bed requires a high-power manmade UV source. The energy savings are self-evident.

Received: September 18, 2012

Accepted: October 30, 2012

Published: October 30, 2012

There are various ways of depositing fine  $\text{TiO}_2$  powder onto a substrate. Nonvacuum methods include doctor blading,<sup>31</sup> dip coating,<sup>32</sup> spin coating,<sup>33</sup> screen printing,<sup>34</sup> and sol-gel<sup>35</sup> approaches, whereas vacuum-based methods include chemical vapor deposition,<sup>36</sup> pulsed laser deposition,<sup>37</sup> and sputtering.<sup>38</sup> All of these methods require a high-temperature sintering and postannealing process for film densification and enhancement of the anatase phase, which is essential for an efficient photocatalytic effect. However, high-temperature methods are disadvantageous because of their high energy consumption. Moreover, they prevent the use of roll-to-roll flexible polymer-based substrates, which are used for low-cost mass production for commercialization. A low-temperature and high-speed coating process, such as aerosol deposition (AD), that does not require post processing could facilitate energy-efficient, environmentally friendly, and low-cost production.

AD promotes<sup>39,40</sup> adhesion and cohesion between  $\text{TiO}_2$  powders and substrates by simply impacting dry powder particles onto the substrate to form a dense, nanocrystalline film at low temperature and at a supersonic speed. AD is also attractive because it yields self-assembled “honeycomb” structures within the  $\text{TiO}_2$  film, which promote a high surface-area-to-volume ratio, thereby enhancing the interfacial photocatalytic effect. Ryu et al.<sup>41,42</sup> studied for the first time the MB photodegradation and the antibacterial effect of AD  $\text{TiO}_2$  films. In their subsequent work, they fabricated porous AD  $\text{TiO}_2$  films by aerosol-depositing mixed powders of  $\text{TiO}_2$  and  $\beta$ -tricalcium phosphate (TCP) because as-deposited films are dense, even though they are rough on surface. The  $\beta$ -TCP phase was leached out by chemical etching using HCl aqueous solution. However, the photocatalytic effect via changing roughness of the AD films and the effect of postannealing treatment was not addressed in their studies. Postannealing induces changes in the film’s surface roughness. We have investigated commensurate changes to the number of surviving bacterial colonies and methylene blue decolorization strengths as well as the film characteristics. Clarification regarding the postannealing treatment is important in light of reducing the number manufacturing processes necessary for the functional films.

## 2. EXPERIMENTS

**2.1. Aerosol Deposition.** Figure 1 is a schematic of the AD experimental setup, consisting of a gas tank, fluidized-bed powder feeder, nozzle, vacuum chamber, 2D  $x$ - $y$  stage, booster pump, and vacuum pump. The powder used is composed of 60% anatase and 40% rutile  $\text{TiO}_2$  by weight (Yee Young Cerachem Ltd., Korea); the composition is easily altered during AD by changing mixture percentages. A 100% anatase powder would have improved photokilling or photodegradation activity. Anatase–rutile mixture powder was used here to ensure low-cost film production. Schlieren images showing the presence of shock waves at the nozzle exit confirmed supersonic gas speeds (not shown here).<sup>43,44</sup> Experimental details of AD are found in our previous studies.<sup>43,44</sup>

Figure 2(a) shows an SEM of a commercially available  $\text{TiO}_2$  powder. Agglomeration is observed. To break up particle clusters, the powder was mixed with water and put into a rotary evaporator, calcined at 400 °C, then ball-milled for 24 h. This break-up process resulted in particles having an average size of approximately 1.0  $\mu\text{m}$ , based on the nanoparticle distribution analyzer (Nanosight, UK). Such pretreated powders are expected to improve the deposition rate.<sup>39</sup> Figure 2(b) shows

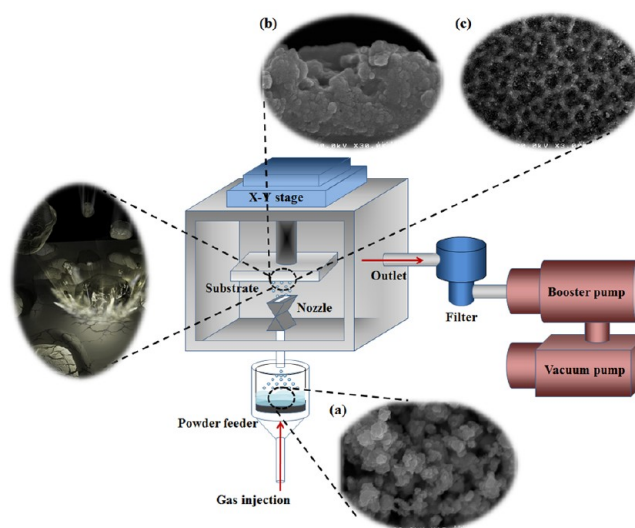


**Figure 1.** Schematic of the experimental setup for the supersonic aerosol deposition system comprising gas tank, fluidized-bed powder feeder, nozzle, vacuum chamber, 2D  $x$ - $y$  stage, booster pump, and vacuum pump. (a) SEM of the  $\text{TiO}_2$  powder (b) side and (c) top views of an AD  $\text{TiO}_2$  film showing the 3D cross-linked honeycomb structure.

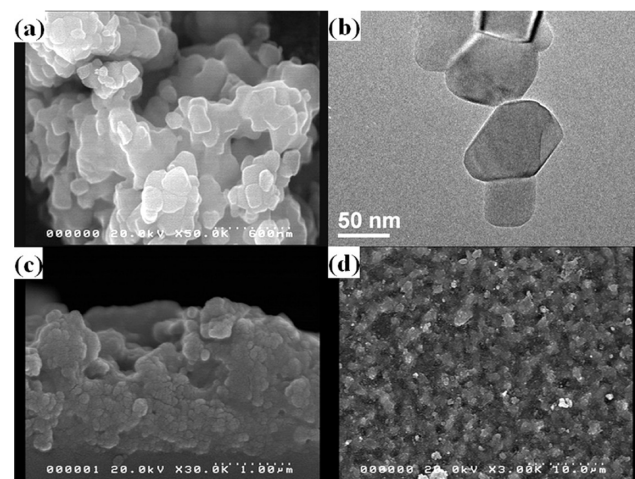


**Figure 2.** (a) SEM image of raw  $\text{TiO}_2$  powder, (b) TEM image of raw single-crystalline  $\text{TiO}_2$  powder, (c) cross-sectional view, and (d) top view of the nanocrystalline  $\text{TiO}_2$  deposited on soda-lime glass using 0.5  $\mu\text{m}$   $\text{TiO}_2$  powder deposited using  $N = 4$  passes and a gas flow of  $Q = 10$  L/min. The film thickness is about 2 mm.

the bright field TEM image of the raw single-crystalline  $\text{TiO}_2$  powder. The crystalline grain size is approximately in the range of 80–100 nm. In Table 1, we show that the grain size of the deposited particles is smaller than the size of the raw powder, which is in the range of 13–20 nm, due to the fracture of the deposited particles at extremely high impact velocity.

Figures 2(c) and (d) are side and top views of the  $\text{TiO}_2$  film, respectively. The side view shows the undulation of the uneven surface, which is desirable for maximizing the photocatalytic interfacial area. The top-view shows the honeycomb structure, which is typical of aerosol-deposited  $\text{TiO}_2$  films.<sup>45,46</sup>

**2.2. Thin Film Characterization.** All  $\text{TiO}_2$  films were manufactured at room temperature on soda-lime glass substrates with surface area and roughness of  $2.5 \times 7.5 \text{ cm}^2$  and  $R_a < 0.1$  nm, respectively. Substrates were cleaned in an

**Table 1. Crystal Sizes of the As-Deposited Film and Annealed Films at Various Temperatures**

	phase	crystal size [nm]
raw-powder	anatase(101)	68.9
	rutile(110)	83.1
as-deposited	anatase(101)	13.8
	rutile(110)	15.7
400 °C	anatase(101)	17.5
	rutile(110)	19.2
500 °C	anatase(101)	18.1
	rutile(110)	16.7
600 °C	anatase(101)	17.2
	rutile(110)	17.7

ultrasonic acetone bath for 10 min before use. The microstructures and crystallinity of the deposited TiO<sub>2</sub> films were characterized by both high-resolution scanning electron microscopy (SEM, Hitachi S-5000) and X-ray diffraction (XRD, Rigaku Japan D/MAX-2500) using Cu K $\alpha$  radiation over a  $2\theta$  range of 20–50°. Atomic force microscopy (AFM, Park Systems XE-100) was used to measure the surface roughness of the substrate and films.

**2.3. Photokilling Activity.** The photokilling activity of the UV-illuminated TiO<sub>2</sub> film was tested using the antibacterial drop test (Figure 3). The entire process was carried out inside

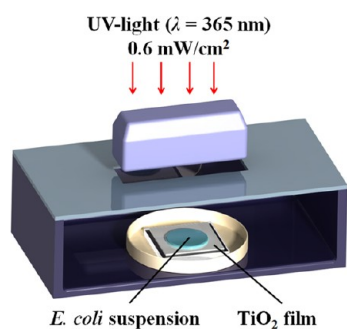


**Figure 3.** Schematic of the photokilling activity experimental setup using the antibacterial drop test. The entire antibacterial test was carried out inside an evacuated glovebox to avoid any possible contamination.

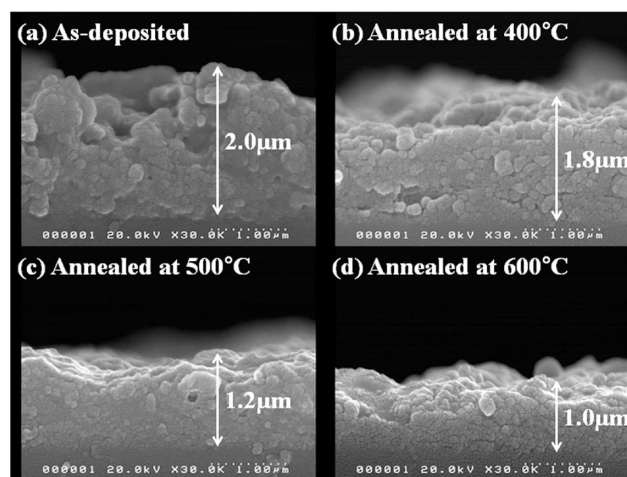
an evacuated glovebox. The TiO<sub>2</sub> films were stored in a dark box for 24 h to minimize possible photocatalytic activity prior to the antibacterial tests. All films were cleaned with an alcohol-soaked tissue prior to the antibacterial test. *E. coli* bacterial colonies were cultivated in a nutrient broth at 37 °C for 24 h. Bacterial colony concentration was controlled by adjusting the amount of solvent. Concentrations of  $2 \times 10^8$  CFU/mL were measured at 600 nm with a spectrophotometry. A centrifuge operating at 3000 rpm for 10 min collected the bacterial cells. The solvent (supernatant) was removed and the separated cells were washed with phosphate buffered saline (PBS) solution twice. The residue was resuspended with PBS solution to adjust the final concentration of bacterial cells to approximately  $2 \times 10^6$  CFU/mL. About 100  $\mu$ L of the final *E. coli* solution was randomly dropped on the substrate in a Petri dish, which was kept inside a dark box. After an hour of weak UV exposure (0.6 mW/cm<sup>2</sup>, 365 nm), about 10 mL of PBS solution was poured onto the film in the Petri dish and mixed with the 100  $\mu$ L *E. coli* solution. The mixture (bacteria suspension) was collected in a conical tube. About 100  $\mu$ L of this bacteria suspension was

placed on a nutrient agar plate. The number of surviving bacterial colonies on the Petri dish was counted after incubation for 24 h at 37 °C. Uncoated glass was also tested as a negative control. The inhibition rate (%) was calculated by comparing colony counts between the tests and control.

**2.4. Photodegradation of Methylene Blue (MB).** Methylene blue (MB) solution is often used as a model pollutant as it decomposes by direct oxidation and from OH radicals generated during the photocatalytic process.<sup>47,48</sup> MB solution (#M2661, 0.1 wt % solution in water, Samchun Chemical, Korea) was mixed with deionized water at a 1:400 volume ratio. A TiO<sub>2</sub> film was placed inside a Pyrex vessel and sealed with a Pyrex Petri dish. The concentration of MB inside the vessel decreased as photocatalysis proceeded; its concentration was monitored by using a UV-Vis spectrophotometer (OPTIZEN POP, Mecasys Co. LTD, Korea,  $190 \leq \lambda \leq 1100$  nm). Absorbance data from the UV-vis spectroscopy was obtained by converting the transmittance data using the Beer–Lambert law<sup>49,50</sup>

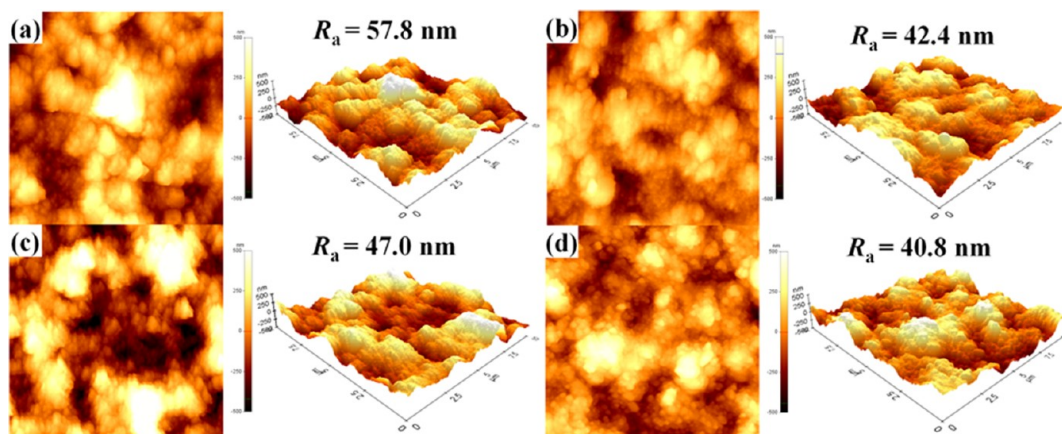
### 3. RESULTS AND DISCUSSION

Figure 4 shows cross-sectional micrographs of pure TiO<sub>2</sub> films deposited on soda-lime glass substrate at various annealing



**Figure 4.** SEM cross-sectional micrographs of dense TiO<sub>2</sub> films on a soda-lime glass: (a) as deposited and annealed at (b) 400, (c) 500, (d) 600 °C.

temperatures, for as-deposited film at room-temperature and films annealed at 400, 500, and 600 °C. The initial thickness of all films was about 2  $\mu$ m before annealing, and the thickness decreases with increasing annealing temperature. There is a slight difference in the microstructures of the films; the grain size decreases, which is consistent with the results of Linderback et al.<sup>51</sup> The density increases commensurately because there is no loss of mass with the decrease in film thickness. The grain sizes ranged from 100 to 200 nm and are homogeneous with depth in the film. Energy dispersive spectroscopic analyses confirmed the homogeneous microstructure of all of the films, which are only composed of titanium and oxygen and have no impurities. All of these films are sufficiently dense to be impermeable; they are not considered porous films. Nevertheless, all films retain highly rough honeycomb structures even after film densification through annealing. Comparing side-views, surface asperities are largest for the as-deposited film. It is well-known that



**Figure 5.** AFM top view images (left) and 3D images (right) of  $\text{TiO}_2$  films: (a) as-deposited and annealed at (b) 400, (c) 500, and (d) 600 °C.

photocatalytic activity increases with increasing surface area. Because of the large surface asperities of the as-deposited film, its photocatalytic activity should be the largest of all films. Some have purposely added Ag-dopant to enhance roughness thereby increasing the interfacial photocatalytic area.<sup>52</sup> Of course, doping Ag can also yield an additional effect of antibacterial activity.

Figure 5 shows the variation in surface roughnesses of the  $\text{TiO}_2$  films shown in Figure 4(a)–(d), which corresponds to the roughness of as-deposited film at room temperature and films annealed at 400, 500, and 600 °C, respectively. The left and right AFM images show the 2D plan- and 3D angle-views of the films, respectively. The 2D images illustrate grain-size reduction, whereas the 3D images demonstrate that all of the films retain a “hill-valley” surface roughness attributed to the honeycomb structure of Figure 1(c) or 2(d). These roughened surface profiles are consistent with the SEM images shown in Figure 4 and are favorable for antibacterial applications, because the increased interfacial surface area maximizes photocatalytic effects. Figure 5 again shows how annealing causes film densification, film thinning, and grain-size reduction (decreased overall surface roughness). However, it cannot be concluded that a higher annealing temperature causes monotonic surface smoothing because the film annealed at 500 °C in Figure 5(c) has a greater surface roughness than the film annealed at 400 °C in Figure 5(b). An amorphous phase does not seem to be present in any of the films, thus annealing does not seem to be necessary for phase transformation.

Figure 6 shows the X-ray diffraction (XRD) patterns of the AD  $\text{TiO}_2$  films (2  $\mu\text{m}$  thick) annealed at 400, 500, and 600 °C to quantify the crystalline phases of the as-deposited and annealed films at various annealing temperatures ( $T_a$ ). Because the annealing temperature needs to be at least 900 °C to transform the anatase phase to rutile  $\text{TiO}_2$ ,<sup>53,54</sup> phase transformation is not expected for  $T_a \leq 600$  °C. Note that the anatase-to-rutile transformation temperature can be lowered with silver doping.<sup>55</sup> The XRD pattern of the raw powder corresponds to 60% anatase and 40% rutile by weight. The peaks at  $2\theta = 25.24^\circ$  and  $2\theta = 27.46^\circ$  represent anatase and rutile, respectively.<sup>56</sup> The diffraction pattern of the as-deposited film shows significant decreases in peak intensity, although these intensities increase as the film undergoes annealing. The ratio of anatase-to-rutile peaks varies from 1.25, 1.1, 1.05, to 1.1 for as-deposited, 400, 500, and 600 °C measurements, respectively. The variation in these ratios is

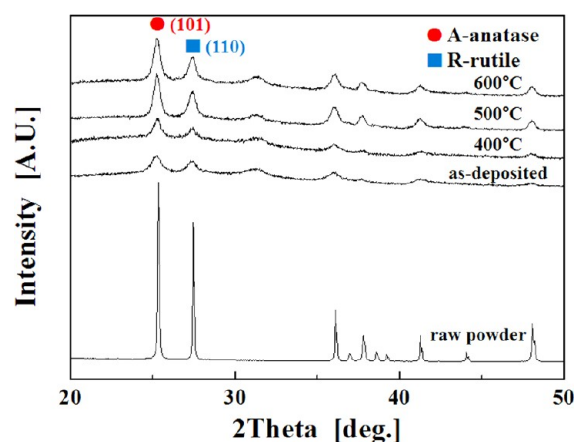


**Figure 6.** XRD patterns of  $\text{TiO}_2$  films: as-deposited and annealed at 400, 500, and 600 °C.

reasonably small, and formation of an amorphous phase is thus unlikely. The decrease in anatase-to-rutile ratio with increasing annealing temperature indicates a slight reduction in the anatase phase. This trend indicates that annealing may not be desirable, because in general, the anatase phase has a higher propensity to enhance photokilling activity. This is an important observation in light of the fact that annealing does not enhance film crystallinity.

The peaks of the AD film are broader and less intense than those of the raw powder, indicating smaller grains, which is consistent with the SEM and AFM images from Figures 4 and 5. However, peak sharpening with increased annealing temperature indicates grain growth and increased crystallinity. The Debye–Scherrer relation states that broad XRD peaks imply smaller grain size,<sup>57,58</sup> consistent with what is expected from AD.<sup>40,41</sup> Residual stresses in the nanosized grains cause shifts in the position of the XRD peaks, but no significant shifts in the peak positions were observed, indicating no residual stresses. Table 1 summarizes the crystal sizes of the as-deposited film and the films annealed at various temperatures. The crystal size variation with increasing annealing temperature is rather random and negligible. Thus the crystal size variation being responsible for the apparent difference shown in the photocatalytic performance of the AD films is highly unlikely.

Figure 7 displays photographs of the bactericidal-test Petri dishes with *E. coli* colonies (white spots) for the as-deposited  $\text{TiO}_2$  films. Photokilling activity was measured by comparing

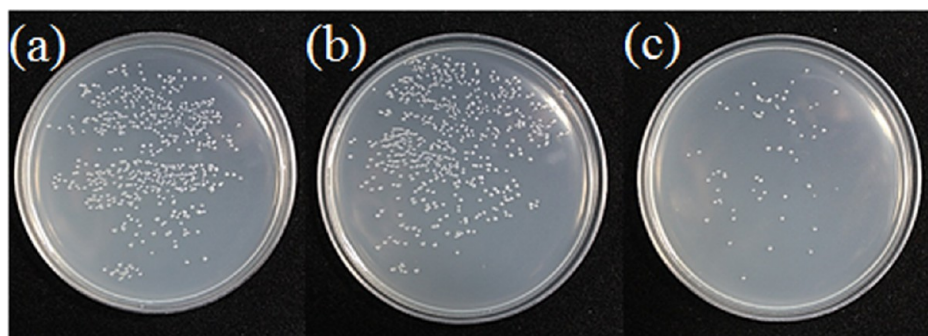


**Figure 7.** Photographs of the bactericidal-test Petri dishes showing the number of surviving *E. coli* colonies on (a) glass without UV-light, (b) glass with 1 h UV exposure, and an (c) as-deposited TiO<sub>2</sub> film after 1 h UV exposure.

the number of surviving *E. coli* bacteria colonies on the coated and uncoated substrates. Three cases are considered: (a) a case without TiO<sub>2</sub> coating and no UV light, (b) a case without TiO<sub>2</sub> coating with UV light, and (c) a case with TiO<sub>2</sub> coating and with UV light. Because UV exposure without TiO<sub>2</sub> photocatalysis is capable of killing bacteria, the effect of UV illumination alone must also be quantified. Note that even with TiO<sub>2</sub> film kept inside a dark box, some photokilling activity was observed because of the presence of the anatase phase and inability to completely eliminate UV exposure, which was also observed by others.<sup>52,59–62</sup>

The effect of UV light alone is quantified by comparing Figures 7(a) and (b); there was no appreciable photokilling activity of the UV-light (at a 15 cm illumination distance and  $\lambda = 365$  nm, UV intensity is 0.6 mW/cm<sup>2</sup>), as the number of surviving bacterial colonies was unchanged. This result confirms that our weak UV-light alone is not capable of inducing antibacterial activity, nor is it capable of directly decomposing MB solution. Comparing Figures 7(b) and (c) shows TiO<sub>2</sub>'s photokilling activity. After 1 h of UV illumination, nearly 90% photokilling activity was observed. After 90 min of UV illumination, 100% photokilling activity was achieved (not shown here). A detailed explanation of photokilling activity for *E. coli* cells was presented by Sunada et al.<sup>63</sup> They explained that the *E. coli* cell wall acts as an outer barrier that hinders initial photokilling. The process is described as a two-step decay chain for the survival rate of *E. coli* on a TiO<sub>2</sub> film.<sup>64</sup>

Figure 8 quantitatively compares the number of surviving *E. coli* bacteria colonies after 1 h of UV illumination for the as-deposited TiO<sub>2</sub> film (far left) and the films annealed at different temperatures. The as-deposited film had the highest photokilling activity. The antibacterial performance of the as-deposited film is expected because it was roughest, yielding the largest interfacial photocatalytic area. The antibacterial performance shown in Figure 8 parallels the surface roughnesses listed in Figure 5. This suggests the dominant role of surface roughness on the antibacterial performance of AD TiO<sub>2</sub> films. Phase transformation or crystallization through annealing was, in fact, counter to antibacterial activity because annealing reduces film roughness. This bodes well for low-cost AD technologies because their post-processing is not required to produce efficient functional TiO<sub>2</sub> films.

Figure 8 also compares the antibacterial performance of films manufactured by RF magnetron cosputtering.<sup>65</sup> The cosputtered films were annealed at 400, 500, and 550 °C, which was analogous to the conditions used to manufacture our AD films. In addition, an 80 W mercury UV lamp was used to illuminate the cosputtered films at room temperature for 1 h; our UV

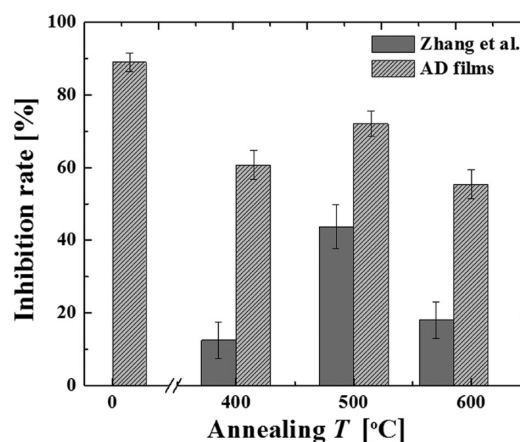


**Figure 8.** Relative number of surviving *E. coli* bacteria colonies after 1 h of UV exposure for an as-deposited TiO<sub>2</sub> film (far left) and the films annealed at increasing temperatures. The results of Zhang et al.<sup>65</sup> are also presented for comparison.

lamp had only a 6 W maximum power. This demonstrates the superiority of room-temperature AD; it requires neither postannealing nor high-powered UV sources. It is worth noting that our photokilling rate was quantified with the aforementioned two-step decay process model.<sup>63,66,67</sup> Single-step, pseudo first-order kinetic models<sup>63,68–70</sup> could not be used because our data are limited to 1 h UV exposures and the bacterial colony time-series evolution with respect to UV duration was not reported by Zhang et al.<sup>71</sup>

Figure 9 displays the effect of UV exposure on MB photodegradation in terms of absorbance data over a wavelength range of 300–800 nm for various UV durations;  $t_{UV} = 0, 1, 2,$  and 3 h; the UV intensity is 0.6 mW/cm<sup>2</sup>, whereas that of Ryu et al.<sup>41</sup> was 10 mW/cm<sup>2</sup>. Greater the intensity of the transmitted light corresponds to lower absorbance, and lower absorbance is indicative of increased photodegradation of the MB solution. The as-deposited film was used because it had the best photocatalytic effect with the highest surface roughnesses, as indicated in Figure 8. The inset figure of Figure 9 is a snapshot of the photoinduced degradation of the MB solution corresponding to the quantitative data in Figure 9. The far-left snapshot shows a nearly transparent MB solution, which indicates a successful water purification process. The highest absorbance peak is observed at  $\lambda \approx 664$  nm,<sup>50</sup> which decreases as the photocatalytic reaction proceeded with  $t_{UV}$ . Peak reduction is caused by the photo-oxidative *N*-demethylation of MB.<sup>71,72</sup> Table 2 compares the reduction of total organic carbon (TOC, Shimadzu TOC-VCSN analyzer)

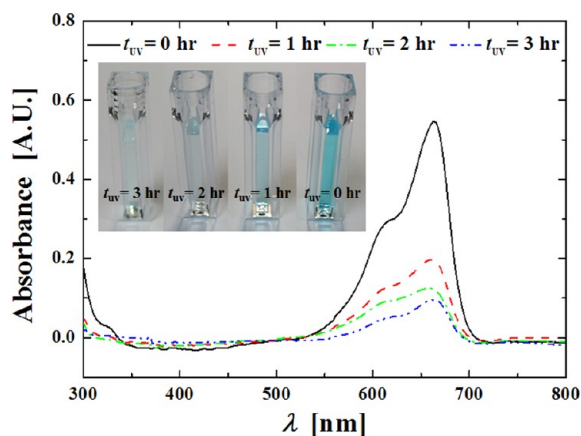


**Figure 9.** Effect of UV exposure on MB photodegradation. UV-vis spectra of the MB solution (0.1 wt % solution in deionized water) with the as-deposited TiO<sub>2</sub> film irradiated for 0, 1, 2, and 3 h (0.6 mW/cm<sup>2</sup> UV exposure in 22 °C air with relative humidity at 80%).

of the as-deposited film and the annealed film at 600 °C. The total organic carbon (TOC) is the amount of carbon bound in an organic compound, which was estimated by subtracting the inorganic carbon (IC) from the total carbon (TC). IC represents the content of dissolved carbon dioxide and carbonic acid salts, whereas TOC is used as a measure of mineralization or water quality. It is clear that TOC reduction is greater for the as-deposited film (84%) than for the annealed film (68%) with respect to TOC of initial concentration of MB. This data indicates that the higher roughness of the as-deposited film is indeed capable of yielding greater photodecomposition activity.

We have, so far, demonstrated the excellent photocatalytic activity of AD TiO<sub>2</sub> films, which increases with surface roughness. To further illustrate this point, we increased the film surface roughness by controlling the operation parameters of AD (i.e., the number of nozzle passes,  $N = 4-6$  and 8). The film surface roughness increased with  $N$ , as evidenced by SEM and AFM images in Figure 10, from  $R_a = 57.8, 80.9,$  and 103.6 nm, respectively. The photodegradation activities of these films ( $N = 4, 6,$  and 8) are compared in Figure 11. All of the films

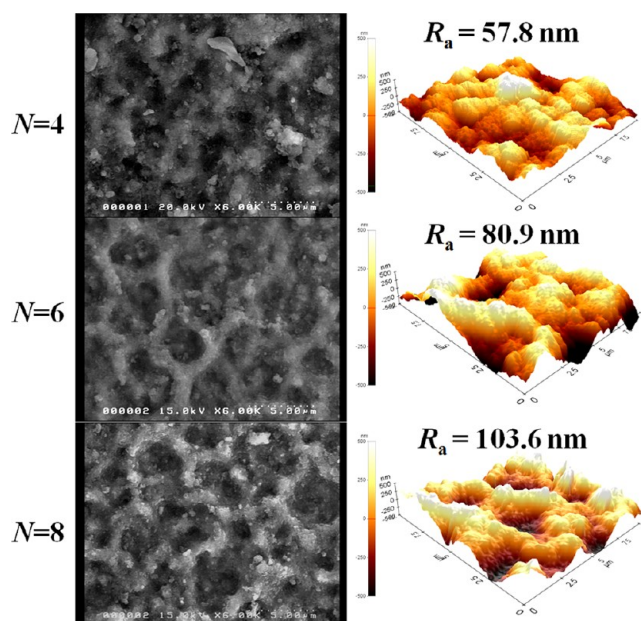


**Figure 10.** Effect of number of passes ( $N$ ) on the film surface roughness from SEM and AFM images. Increasing  $N$  yields a rougher surface morphology.

used in Figure 11 are the as-deposited. The UV exposure time was 1 h. The film with the highest roughness ( $N = 8$ ) yielded the best photodegradation activity as its absorbance curve (indicated by the blue dashed-line) was flattest in Figure 11. Decolorization snapshots in the inset also show that  $N = 8$  has the highest photodegradation activity. As such, the increased roughness of AD TiO<sub>2</sub> films increased both the photokilling of *E. coli* and the photodegradation of MB. This simple and rapid AD method facilitates the mass production of low-cost antibacterial TiO<sub>2</sub> films for a wide range of industrial applications such as environmental cleanup and biomedical membranes, with potential for mass roll-to-roll production.

**Table 2. Comparison for the Reduction of Total Organic Carbon (TOC, Shimadzu TOC-VCSN Analyzer) of the As-Deposited Film and the Annealed Film at 600 °C**

	test	unit	MDL	total carbon (TC)	inorganic carbon (IC)	TOC (TC-IC)	dilution amount	final TOC
MB	RUN1	mg/L	0.01	5.67	0.17	5.50	20	109.94
	RUN2	mg/L	0.01	5.70	0.17	5.53	20	110.60
	std dev			0.02	0.00			
	coefficient of variation			0.37	1.24			
	avg	mg/L	0.01	5.69	0.17	5.51	20	110.27
As-deposited film	RUN1	mg/L	0.01	1.09	0.20	0.89	20	17.82
	RUN2	mg/L	0.01	1.08	0.20	0.88	20	17.60
	std dev			0.01	0.00			
	coefficient of variation			0.98	1.41			
	avg	mg/L	0.01	1.09	0.20	0.89	20	17.71
film annealed at 600 °C	RUN1	mg/L	0.01	1.95	0.22	1.73	20	34.60
	RUN2	mg/L	0.01	1.96	0.22	1.74	20	34.88
	std dev			0.01	0.00			
	coefficient of variation			0.58	0.65			
	avg	mg/L	0.01	1.95	0.22	1.74	20	34.74

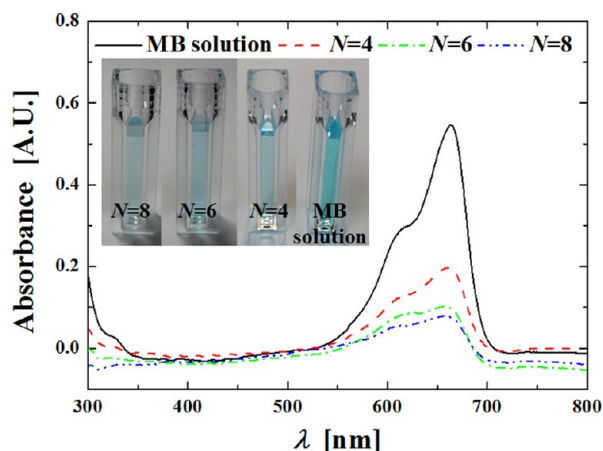


**Figure 11.** Effect of surface roughness ( $N = 4, 6,$  and  $8$ ) for as-deposited  $\text{TiO}_2$  films on MB photodegradation after 1 h of UV exposure ( $0.6 \text{ mW/cm}^2$  UV exposure in  $22^\circ\text{C}$  air with relative humidity at  $80\%$ ). UV-vis spectra of the MB solution ( $0.1 \text{ wt } \%$  solution in deionized water) for the various film surface roughnesses indicated in Figure 10. Films coated with  $N = 4, 6,$  and  $8$  yielded the lowest, moderate, and highest photodegradation effect, respectively.

## AUTHOR INFORMATION

### Corresponding Author

\*E-mail: skyoon@korea.ac.kr.

### Notes

The authors declare no competing financial interest.

## ACKNOWLEDGMENTS

This research was supported by World Class University (WCU) program (Case III) through the National Research Foundation of Korea (R33-10046), NRF-2012-0001169, and the Converging Research Center Program through the Ministry of Education, Science and Technology (2010K000969). This work was also supported by Grant Nos. NRF-2011-0030433 and 2010-0010217, funded by the Korean government (MEST) and by a grant from the cooperative R&D Program (B551179-08-03-00) funded by the Korea Research Council Industrial Science and Technology.

## REFERENCES

- (1) Bhatkhande, D. S.; Pangarkar, V. G.; Beenackers, A. A. Photocatalytic degradation for environmental applications—A review. *J. Chem. Technol. Biotechnol.* **2002**, *77* (1), 102–116.
- (2) Fujishima, A.; Honda, K. Photolysis-decomposition of water at the surface of an irradiated semiconductor. *Nature* **1972**, *238* (5385), 37–38.
- (3) Huang, Z.; Maness, P. C.; Blake, D. M.; Wolfrum, E. J.; Smolinski, S. L.; Jacoby, W. A. Bactericidal mode of titanium dioxide photocatalysis. *J. Photochem. Photobiol., A* **2000**, *130* (2), 163–170.
- (4) Kabra, K.; Chaudhary, R.; Sawhney, R. L. Treatment of hazardous organic and inorganic compounds through aqueous-phase photocatalysis: A review. *Ind. Eng. Chem. Res.* **2004**, *43* (24), 7683–7696.
- (5) Jacoby, W. A.; Blake, D. M.; Noble, R. D.; Koval, C. A. Kinetics of the oxidation of trichloroethylene in air via heterogeneous photocatalysis. *J. Catal.* **1995**, *157* (1), 87–96.
- (6) Obee, T. N. Photooxidation of sub-parts-per-million toluene and formaldehyde levels on titania using a glass-plate reactor. *Environ. Sci. Technol.* **1996**, *30* (12), 3578–3584.
- (7) Davis, R. J.; Gainer, J. L.; O'Neal, G.; Wu, I. W. Photocatalytic decolorization of wastewater dyes. *Water Environ. Res.* **1994**, *66* (1), 50–53.

- (8) Tanaka, K.; Padermpole, K.; Hisanaga, T. Photocatalytic degradation of commercial azo dyes. *Water Res.* **2000**, *34* (1), 327–333.

- (9) Wang, Y. Solar photocatalytic degradation of eight commercial dyes in  $\text{TiO}_2$  suspension. *Water Res.* **2000**, *34* (3), 990–994.

- (10) Li, X.; Yue, P.; Mak, C. Photooxidation of wool dye and TCP in aqueous solution using an innovative  $\text{TiO}_2$  mesh electrode. *Water Sci. Technol.* **2000**, *42* (12), 181–188.

- (11) Sakthivel, S.; Neppolian, B.; Palanichamy, M.; Arabindoo, B.; Murugesan, V. Photocatalytic degradation of leather dye over ZnO catalyst supported on alumina and glass surfaces. *Water Sci. Technol.* **2001**, 211–218.

- (12) Arslan, I.; Baicioglu, I.; Bahnemann, D. Photochemical treatment of simulated dyehouse effluents by novel  $\text{TiO}_2$  photocatalysts: Experience with the thin film fixed bed (TFFB) and double skin sheet (DSS) reactor. *Water Sci. Technol.* **2001**, 171–178.

- (13) Tseng, J.; Huang, C. Removal of chlorophenols from water by photocatalytic oxidation. *Water Sci. Technol.* **1991**, *23* (1–3), 377–387.

- (14) Blake, D. M.; Webb, J.; Turchi, C.; Magrini, K. Kinetic and mechanistic overview of  $\text{TiO}_2$ -photocatalyzed oxidation reactions in aqueous solution. *Solar Energy Mater.* **1991**, *24* (1–4), 584–593.

- (15) Suri, R. P. S.; Liu, J.; Hand, D. W.; Crittenden, J. C.; Perram, D. L.; Mullins, M. E. Heterogeneous photocatalytic oxidation of hazardous organic contaminants in water. *Water Environ. Res.* **1993**, *65* (5), 665–673.

- (16) Sherrard, K. B.; Marriott, P. J.; Amiet, R. G.; Colton, R.; McCormick, M. J.; Smith, G. C. Photocatalytic degradation of secondary alcohol ethoxylate: Spectroscopic, chromatographic, and mass spectrometric studies. *Environ. Sci. Technol.* **1995**, *29* (9), 2235–2242.

- (17) Hamerski, M.; Grzechulska, J.; Morawski, A. W. Photocatalytic purification of soil contaminated with oil using modified  $\text{TiO}_2$  powders. *Solar Energy* **1999**, *66* (6), 395–399.

- (18) Blake, D. M.; Maness, P. C.; Huang, Z.; Wolfrum, E. J.; Huang, J.; Jacoby, W. A. Application of the photocatalytic chemistry of titanium dioxide to disinfection and the killing of cancer cells. *Sep. Purif. Methods* **1999**, *28* (1), 1–50.

- (19) Jimmy, C. Y.; Ho, W.; Lin, J.; Yip, H.; Wong, P. K. Photocatalytic activity, antibacterial effect, and photoinduced hydrophilicity of  $\text{TiO}_2$  films coated on a stainless steel substrate. *Environ. Sci. Technol.* **2003**, *37* (10), 2296–2301.

- (20) Huang, Z.; Maness, P.-C.; Blake, D. M.; Wolfrum, E. J.; Smolinski, S. L.; Jacoby, W. A. Bactericidal mode of titanium dioxide photocatalysis. *J. Photochem. Photobiol., A* **2000**, *130* (2–3), 163–170.

- (21) Kang, Q.; Lu, Q. Z.; Liu, S. H.; Yang, L. X.; Wen, L. F.; Luo, S. L.; Cai, Q. Y. A ternary hybrid  $\text{CdS/Pt-TiO}_2$  nanotube structure for photoelectrocatalytic bactericidal effects on *Escherichia Coli*. *Biomaterials* **2010**, *31* (12), 3317–3326.

- (22) Lin, H.; Xu, Z.; Wang, X.; Long, J.; Su, W.; Fu, X.; Lin, Q. Photocatalytic and antibacterial properties of medical grade PVC material coated with  $\text{TiO}_2$  film. *J. Biomed. Mater. Res., Part B* **2008**, *87* (2), 425–431.

- (23) Richardson, S. D.; Thruston, A. D., Jr; Collette, T. W.; Patterson, K. S.; Lykins, B. W., Jr; Ireland, J. C. Identification of  $\text{TiO}_2$ /UV disinfection byproducts in drinking water. *Environ. Sci. Technol.* **1996**, *30* (11), 3327–3334.

- (24) Eggins, B. R.; Palmer, F. L.; Byrne, J. A. Photocatalytic treatment of humic substances in drinking water. *Water Res.* **1997**, *31* (5), 1223–1226.

- (25) Fujishima, A.; Rao, T. N.; Tryk, D. A. Titanium dioxide photocatalysis. *J. Photochem. Photobiol., C* **2000**, *1* (1), 1–21.

- (26) Li, C.; Li, W. Deposition characteristics of titanium coating in cold spraying. *Surf. Coat. Technol.* **2003**, *167* (2–3), 278–283.

- (27) Haarstrick, A.; Kut, O.; Heinzle, E.  $\text{TiO}_2$ -assisted degradation of environmentally relevant organic compounds in wastewater using a novel fluidized bed photoreactor. *Environ. Sci. Technol.* **1996**, *30* (3), 817–824.

- (28) Ochuma, I. J.; Osibo, O. O.; Fishwick, R. P.; Pollington, S.; Wagland, A.; Wood, J.; Winterbottom, J. M. Three-phase photocatalysis using suspended titania and titania supported on a reticulated foam monolith for water purification. *Catal. Today* **2007**, *128* (1–2), 100–107.
- (29) Matos, J.; Laine, J.; Herrmann, J. M. Synergy effect in the photocatalytic degradation of phenol on a suspended mixture of titania and activated carbon. *Appl. Catal., B* **1998**, *18* (3–4), 281–291.
- (30) Beydoun, D.; Amal, R.; Scott, J.; Low, G.; McEvoy, S. Studies on the mineralization and separation efficiencies of a magnetic photocatalyst. *Chem. Eng. Technol.* **2001**, *24* (7), 745–748.
- (31) Nazeeruddin, M. K.; Kay, A.; Rodicio, I.; Humphry-Baker, R.; Müller, E.; Liska, P.; Vlachopoulos, N.; Grätzel, M. Conversion of light to electricity by cis-X<sub>2</sub>bis (2, 2'-bipyridyl-4, 4'-dicarboxylate) ruthenium (II) charge-transfer sensitizers (X= Cl-, Br-, I-, CN-, and SCN-) on nanocrystalline titanium dioxide electrodes. *J. Am. Ceram. Soc.* **1993**, *115* (14), 6382–6390.
- (32) Sawunyama, P.; Jiang, L.; Fujishima, A.; Hashimoto, K. Photodecomposition of a Langmuir-Blodgett film of stearic acid on TiO<sub>2</sub> film observed by in situ atomic force microscopy and FT-IR. *J. Phys. Chem. B* **1997**, *101* (51), 11000–11003.
- (33) Tatsuma, T.; Kubo, W.; Fujishima, A. Patterning of solid surfaces by photocatalytic lithography based on the remote oxidation effect of TiO<sub>2</sub>. *Langmuir* **2002**, *18* (25), 9632–9634.
- (34) Cheng, L. F.; Wang, Y.; Dai, S. Y.; Wu, Q. C.; Wang, K. J. Preparation and virtues of nanocrystalline TiO<sub>2</sub> porous film and its application in solar cell. *Chin. J. Mater. Res.* **1996**, *10*, 404.
- (35) Wang, Z.; Helmersson, U.; Käll, P.-O. Optical properties of anatase TiO<sub>2</sub> thin films prepared by aqueous sol-gel process at low temperature. *Thin Solid Films* **2002**, *405* (1–2), 50–54.
- (36) Campbell, S.; Kim, H. S.; Gilmer, D.; He, B.; Ma, T.; Gladfelter, W. Titanium dioxide (TiO<sub>2</sub>)-based gate insulators. *IBM J. Res. Dev.* **1999**, *43* (3), 383–392.
- (37) Kim, J.-H.; Lee, S.; Im, H.-S. The effect of target density and its morphology on TiO<sub>2</sub> thin films grown on Si(100) by PLD. *Appl. Surf. Sci.* **1999**, *151* (1–2), 6–16.
- (38) Tang, H.; Prasad, K.; Sanjines, R.; Schmid, P.; Levy, F. Electrical and optical properties of TiO<sub>2</sub> anatase thin films. *J. Appl. Phys.* **1994**, *75* (4), 2042–2047.
- (39) Akedo, J. Aerosol deposition of ceramic thick films at room temperature: Densification mechanism of ceramic layers. *J. Am. Ceram. Soc.* **2006**, *89* (6), 1834–1839.
- (40) Akedo, J. Room temperature impact consolidation (RTIC) of fine ceramic powder by aerosol deposition method and applications to microdevices. *J. Therm. Spray Technol.* **2008**, *17* (2), 181–198.
- (41) Ryu, J.; Park, D. S.; Hahn, B. D.; Choi, J. J.; Yoon, W. H.; Kim, K. Y.; Yun, H. S. Photocatalytic TiO<sub>2</sub> thin films by aerosol-deposition: From micron-sized particles to nano-grained thin film at room temperature. *Appl. Catal., B* **2008**, *83* (1–2), 1–7.
- (42) Ryu, J.; Hahn, B.; Choi, J.; Yoon, W.; Lee, B.; Choi, J.; Park, D. Porous Photocatalytic TiO<sub>2</sub> Thin Films by Aerosol Deposition. *J. Am. Ceram. Soc.* **2010**, *93* (1), 55–58.
- (43) Park, J. J.; Lee, M. W.; Yoon, S. S.; Kim, H. Y.; James, S. C.; Heister, S. D.; Chandra, S.; Yoon, W. H.; Park, D. S.; Ryu, J. Supersonic nozzle flow simulations for particle coating applications: Effects of shockwaves, nozzle geometry, ambient pressure, and substrate location upon flow characteristics. *J. Therm. Spray Technol.* **2011**, *20*, 514–522.
- (44) Lee, M.; Park, J.; Kim, D.; Yoon, S.; Kim, H.; Kim, D.; James, S.; Chandra, S.; Coyle, T.; Ryu, J. Optimization of supersonic nozzle flow for titanium dioxide thin-film coating by aerosol deposition. *J. Aerosol Sci.* **2011**, *42* (11), 771–780.
- (45) Park, J. J.; Kim, D. Y.; Lee, J. G.; Kim, H. Y.; Yoon, S. S.; Kim, D.; Oh, J.-H.; Seong, T.-Y.; James, S. C.; van Hest, Maikel F.A.M.; Sanjeev, C. High-transmittance superhydrophilic TiO<sub>2</sub> thin films fabricated by aerosol deposition for self-cleaning applications. *Adv. Funct. Mater.* **2012**.
- (46) Kim, D. Y.; Park, J. J.; Lee, M. W.; Lee, J. G.; Yoon, S. S.; Kim, H. Y.; Oh, J. H.; Seong, T. Y.; Kim, D. H.; Hong, J. I.; James, S. C.; Hest, M. v.; Chandra, S. Hydrophilicity and hydrophobicity of TiO<sub>2</sub> films produced by aerosol deposition. *J. Am. Ceram. Soc.* **2012**, accepted.
- (47) Draper, R. B.; Fox, M. A. Titanium dioxide photosensitized reactions studied by diffuse reflectance flash photolysis in aqueous suspensions of TiO<sub>2</sub> powder. *Langmuir* **1990**, *6* (8), 1396–1402.
- (48) Turchi, C. S.; Ollis, D. F. Mixed reactant photocatalysis: Intermediates and mutual rate inhibition. *J. Catal.* **1989**, *119* (2), 483–496.
- (49) Fuwa, K.; Valle, B. The physical basis of analytical atomic absorption spectrometry. The pertinence of the Beer-Lambert law. *Anal. Chem.* **1963**, *35* (8), 942–946.
- (50) Yogi, C.; Kojima, K.; Wada, N.; Tokumoto, H.; Takai, T.; Mizoguchi, T.; Tamiaki, H. Photocatalytic degradation of methylene blue by TiO<sub>2</sub> film and Au particles-TiO<sub>2</sub> composite film. *Thin Solid Films* **2008**, *516* (17), 5881–5884.
- (51) Linderbäck, P.; Harmankaya, N.; Askendal, A.; Areva, S.; Lausmaa, J.; Tengvall, P. The effect of heat-or ultra violet ozone-treatment of titanium on complement deposition from human blood plasma. *Biomaterials* **2010**, *31* (18), 4795–4801.
- (52) Yu, B.; Leung, K. M.; Guo, Q.; Lau, W. M.; Yang, J. Synthesis of Ag-TiO<sub>2</sub> composite nano thin film for antimicrobial application. *Nanotechnology* **2011**, *22*, 115603.
- (53) Manjubala, I.; Sampath Kumar, T. Effect of TiO<sub>2</sub>-Ag<sub>2</sub>O additives on the formation of calcium phosphate based functionally graded bioceramics. *Biomaterials* **2000**, *21* (19), 1995–2002.
- (54) Ding, Z.; Lu, G.; Greenfield, P. Role of the crystallite phase of TiO<sub>2</sub> in heterogeneous photocatalysis for phenol oxidation in water. *J. Phys. Chem. B* **2000**, *104* (19), 4815–4820.
- (55) Xin, B.; Jing, L.; Ren, Z.; Wang, B.; Fu, H. Effects of simultaneously doped and deposited Ag on the photocatalytic activity and surface states of TiO<sub>2</sub>. *J. Phys. Chem. B* **2005**, *109* (7), 2805–2809.
- (56) Kwak, S. Y.; Kim, S. H.; Kim, S. S. Hybrid organic/inorganic reverse osmosis (RO) membrane for bactericidal anti-fouling. I. Preparation and characterization of TiO<sub>2</sub> nanoparticle self-assembled aromatic polyamide thin-film-composite (TFC) membrane. *Environ. Sci. Technol.* **2001**, *35* (11), 2388–2394.
- (57) Lebedev, M.; Akedo, J.; Iwata, A.; Sugimoto, S.; Inomata, K. NiZnCu ferrite thick film with nano scale crystallites formed by the aerosol deposition method. *J. Am. Ceram. Soc.* **2004**, *87* (9), 1621–1624.
- (58) Birks, L.; Friedman, H. Particle size determination from X-ray line broadening. *J. Appl. Phys.* **1946**, *17* (8), 687–692.
- (59) Mukhopadhyay, A.; Basak, S.; Das, J. K.; Medda, S. K.; Chattopadhyay, K.; De, G. Ag-TiO<sub>2</sub> Nanoparticle Codoped SiO<sub>2</sub> Films on ZrO<sub>2</sub> Barrier-Coated Glass Substrates with Antibacterial Activity in Ambient Condition. *ACS Appl. Mater. Interfaces* **2010**.
- (60) Shah, M. S. A. S.; Nag, M.; Kalagara, T.; Singh, S.; Manorama, S. V. Silver on PEG-PU-TiO<sub>2</sub> polymer nanocomposite films: An excellent system for antibacterial applications. *Chem. Mater.* **2008**, *20* (7), 2455–2460.
- (61) Wu, T. S.; Wang, K. X.; Li, G. D.; Sun, S. Y.; Sun, J.; Chen, J. S. Montmorillonite-supported Ag/TiO<sub>2</sub> nanoparticles: An efficient visible-light bacteria photodegradation material. *ACS Appl. Mater. Interfaces* **2010**, *2* (2), 544–550.
- (62) Chen, S. F.; Li, J. P.; Qian, K.; Xu, W. P.; Lu, Y.; Huang, W. X.; Yu, S. H. Large scale photochemical synthesis of M@TiO<sub>2</sub> nanocomposites (M= Ag, Pd, Au, Pt) and their optical properties, CO oxidation performance, and antibacterial effect. *Nano Res.* **2010**, *3* (4), 244–255.
- (63) Sunada, K.; Watanabe, T.; Hashimoto, K. Studies on photokilling of bacteria on TiO<sub>2</sub> thin film. *J. Photochem. Photobiol., A* **2003**, *156* (1–3), 227–233.
- (64) Sunada, K.; Watanabe, T.; Hashimoto, K. Bactericidal activity of copper-deposited TiO<sub>2</sub> thin film under weak UV light illumination. *Environ. Sci. Technol.* **2003**, *37* (20), 4785–4789.
- (65) Zhang, H.; Wen, D. Antibacterial properties of Sb-TiO<sub>2</sub> thin films by RF magnetron co-sputtering. *Surf. Coat. Technol.* **2007**, *201* (9–11), 5720–5723.

(66) Tone, S. Kinetic analysis of photochemical sterilization of thermotolerant bacterial spores in slurry of semiconductor catalyst particles with aeration. *Kagaku Kogaku Ronbunshu* **1993**, *19*, 1149–1156.

(67) Horie, Y.; David, D. A.; Taya, M.; Tone, S. Effects of light intensity and titanium dioxide concentration on photocatalytic sterilization rates of microbial cells. *Ind. Eng. Chem. Res.* **1996**, *35* (11), 3920–3926.

(68) Wei, C.; Lin, W. Y.; Zainal, Z.; Williams, N. E.; Zhu, K.; Kruzic, A. P.; Smith, R. L.; Rajeshwar, K. Bactericidal activity of TiO<sub>2</sub> photocatalyst in aqueous media: Toward a solar-assisted water disinfection system. *Environ. Sci. Technol.* **1994**, *28* (5), 934–938.

(69) Watts, R. J.; Kong, S.; Orr, M. P.; Miller, G. C.; Henry, B. E. Photocatalytic inactivation of coliform bacteria and viruses in secondary wastewater effluent. *Water Res.* **1995**, *29* (1), 95–100.

(70) Krýsa, J.; Waldner, G.; Měšťánková, H.; Jirkovský, J.; Grabner, G. Photocatalytic degradation of model organic pollutants on an immobilized particulate TiO<sub>2</sub> layer: Roles of adsorption processes and mechanistic complexity. *Appl. Catal., B* **2006**, *64* (3), 290–301.

(71) Zhang, T.; Oyama, T.; Aoshima, A.; Hidaka, H.; Zhao, J.; Serpone, N. Photooxidative *N*-demethylation of methylene blue in aqueous TiO<sub>2</sub> dispersions under UV irradiation. *J. Photochem. Photobiol., A* **2001**, *140* (2), 163–172.

(72) Sakatani, Y.; Grosso, D.; Nicole, L.; Boissière, C.; de AA Soler-Illia, G. J.; Sanchez, C. Optimised photocatalytic activity of grid-like mesoporous TiO<sub>2</sub> films: Effect of crystallinity, pore size distribution, and pore accessibility. *J. Mater. Chem.* **2006**, *16* (1), 77–82.